Supplementary Figure 1

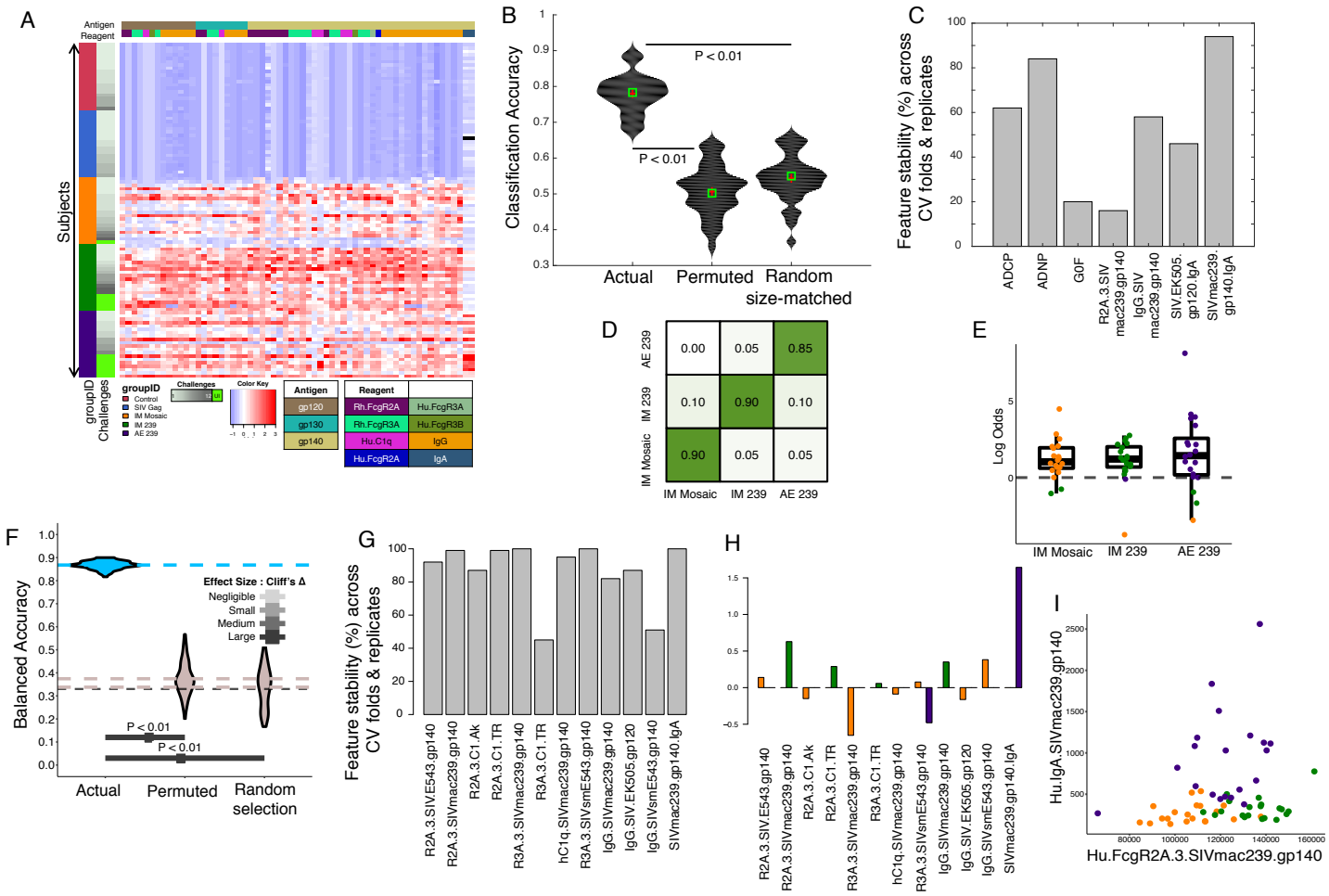

Supplementary Figure 1. Distinct humoral responses are induced in an arm-specific manner, as indicated by supervised and unsupervised analysis. (**A**) Heatmap of Env-specific humoral responses showing their induction among Env-vaccinated (IM mosaic, IM239, AE239 arms) but not other (control, SIV Gag-vaccinated) animals. Each row represents an animal (*n* = 60), color coded by study arm and ordered in ascending order of time-to infection. Each column represents an Fc array measurement, normalized to have zero mean and unit variance. (**B-I**) Classification of Env-vaccinated animals by study arm using LASSO/SVM (**B-C**) and LASSO/logistic regression (**D-I**). (**B**) Comparison of arm classification accuracy among Env-vaccinated animals for the LASSO/SVM model using functional and biophysical data, from cross-validation using actual, permuted and randomly selected (size-matched) humoral features (*n* = 60 animals across three arms; one-sided *P*-value from permutation test, distribution mean and medians are shown as red crosses and green squares respectively). (**C**) The feature frequency (%) across CV folds and replicates for features in the final LASSO/SVM model. (**D**) Confusion matrix of test set predictions from the representative 10-fold cross-validation using logistic regression using all humoral response data. The reverse diagonal shows the proportion of true positive predictions for each adjuvant group. (**E**) Log odds boxplot of predicting the true class label for each animal in the three Env-immunized study arms in the logistic regression. Each animal is colored by its predicted group's color (*n* = 60 animals across three arms). Boxplots depict the median and interquartile range. (**F**) Comparison of logistic regression classification performance from repeated cross-validation using actual versus permuted data and a size-matched random feature set (one-sided *P*-value from control models; effect size: Cliff's Δ, *n* = 100 independent repetitions). (**G**) The feature frequency (%) across CV folds and replicates for features in the final logistic regression model. (**H**) Coefficient weights for the final logistic regression model. (**I**) Biplot visualization of the top two logistic regression coefficients by magnitude.

Supplementary Figure 2

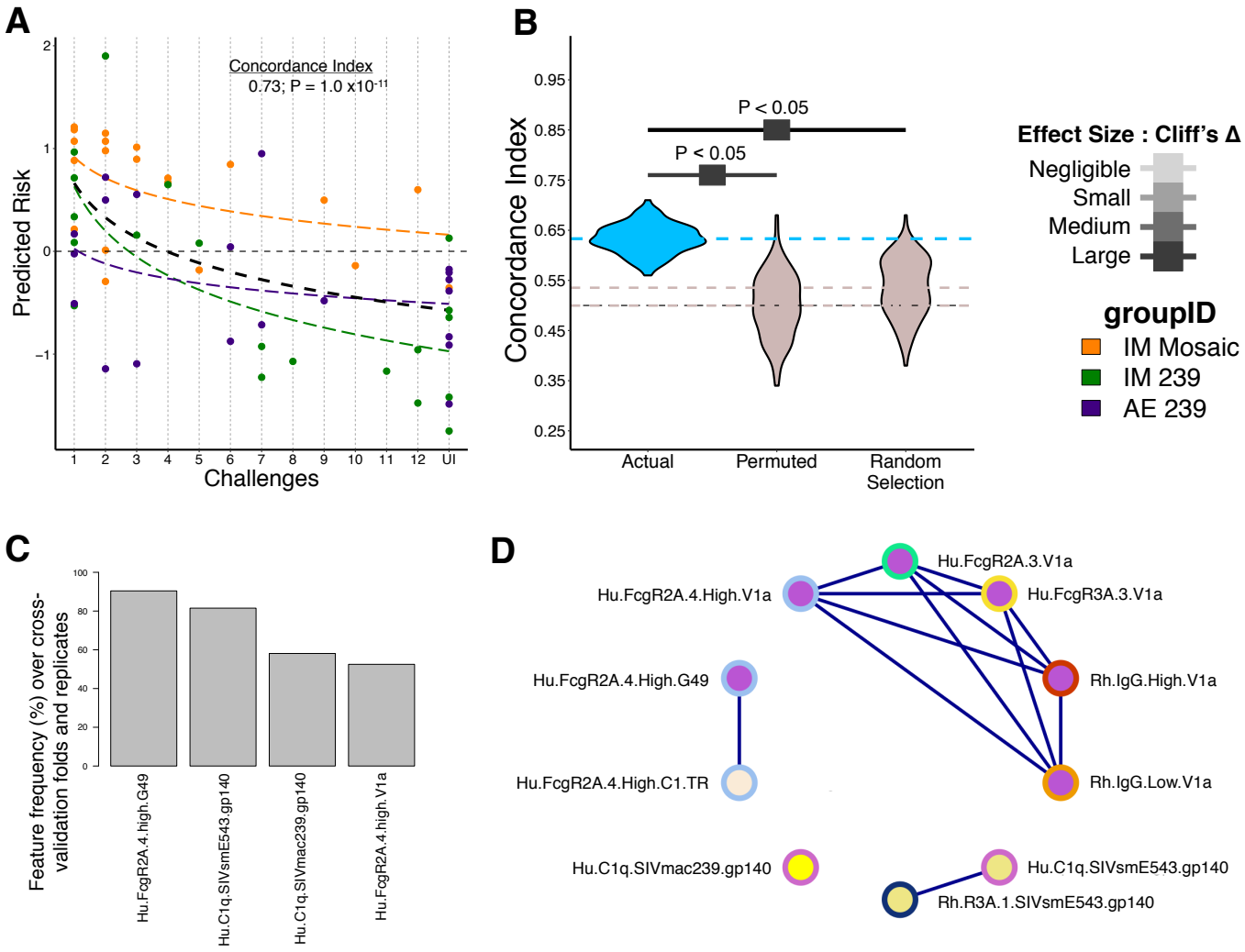

Supplementary Figure 2. Accuracy, robustness, and feature substitution analysis of protection models learned across Env-immunized animals. (**A**) Correlation plot showing the predicted relative risk of infection for each animal in the representative cross-validation test (relative to mean at 0, dashed line) versus the observed per-animal challenge data in CoxPH models. Fit lines approximate relative risk as a log function of time-to-infection. (**B**) Comparison of Concordance index values from repeated 10-fold cross-validation using actual versus permuted and size-matched random feature selection. (*P*-values: probability that control model exceeds actual model performance; effect size: Cliff's Δ; *n* = 100 independent repetitions). The horizontal dashed lines represent the median Concordance indices and the baseline for random prediction (0.5). (**C**) The feature frequency (%) across CV folds and replicates for features in the final model. (**D**) Co-correlates of the features in the final model revealed from substitution analysis. Nodes represent features and edges represent significant correlation (*P*-values < 0.05, Pearson) between them.

Supplementary Figure 3

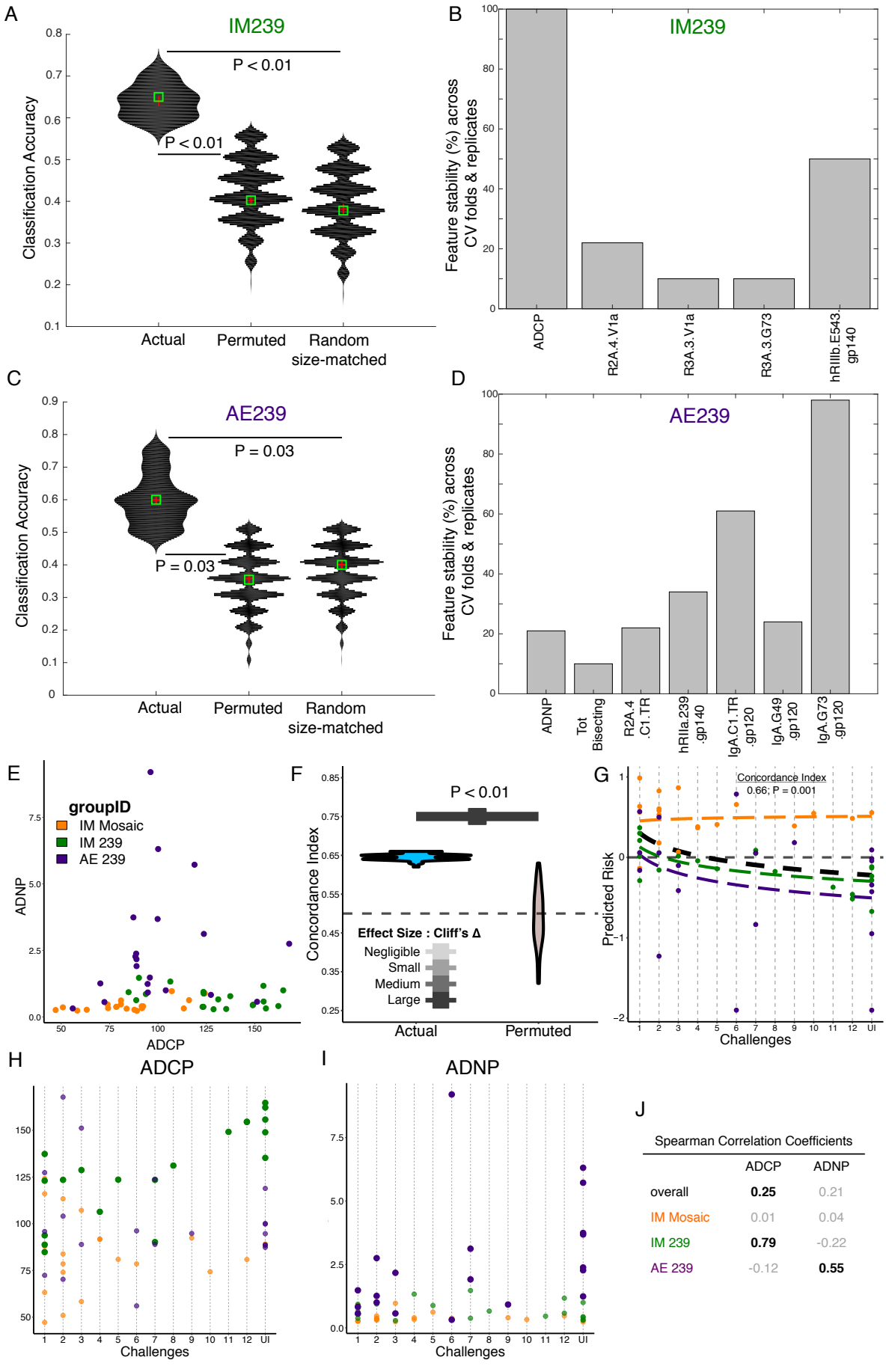

J

Spearman Correlation Coefficients

	ADCP	ADNP
overall	**0.25**	0.21
IM Mosaic	0.01	0.04
IM 239	**0.79**	-0.22
AE 239	-0.12	**0.55**

Supplementary Figure 3. Functional correlates of protection. (**A-D**) Accuracy and robustness of challenge outcome classification LASSO models within IM239 and AE239 study arms. (**A,C**) Comparison of classification accuracy for the classification model for predicting protection status (survived ≤ 4 challenges, survived 5-9 challenges or survived ≥10 challenges) within the IM239 (**A**) and AE239 (**C**) study arms, from repeated cross-validation using actual, permuted, and randomly selected (size-matched) features (n = 20 animals in each of the two arms; one-sided P values from permutation tests, distribution means and medians are shown as red crosses and green squares respectively). (**B,D**) The feature frequency (%) across CV folds and replicates for features in the final model for IM239 (**B**) and AE239 (**D**) study arms. (**E**) Bi-plot of the two phagocytosis functions. (**F-G**) Accuracy and robustness of CoxPH model using phagocysosis features. (**F**) Comparison of C-index values from repeated 10-fold cross-validation using actual versus permuted features. (*P*-values: probability that control model exceeds actual model performance; effect size: Cliff's Δ). (**G**) Correlation plot showing the predicted relative risk of infection for each animal (*n* = 60) in the representative cross-validation test (relative to mean at 0, dashed line) versus the observed per-animal challenge data in CoxPH models. Fit lines approximate relative risk as a log function of time-to-infection. (**H-I**) Correlative relationships between ADCP (**H**) and ADNP (**I**) and challenge outcomes by arm. (**J**) Table provides arm-wise and overall correlation of these functions with protection (Spearman: two-sided *P*-values < 0.05 indicated in bold; *P* = NS indicated in gray).

Supplementary Figure 4

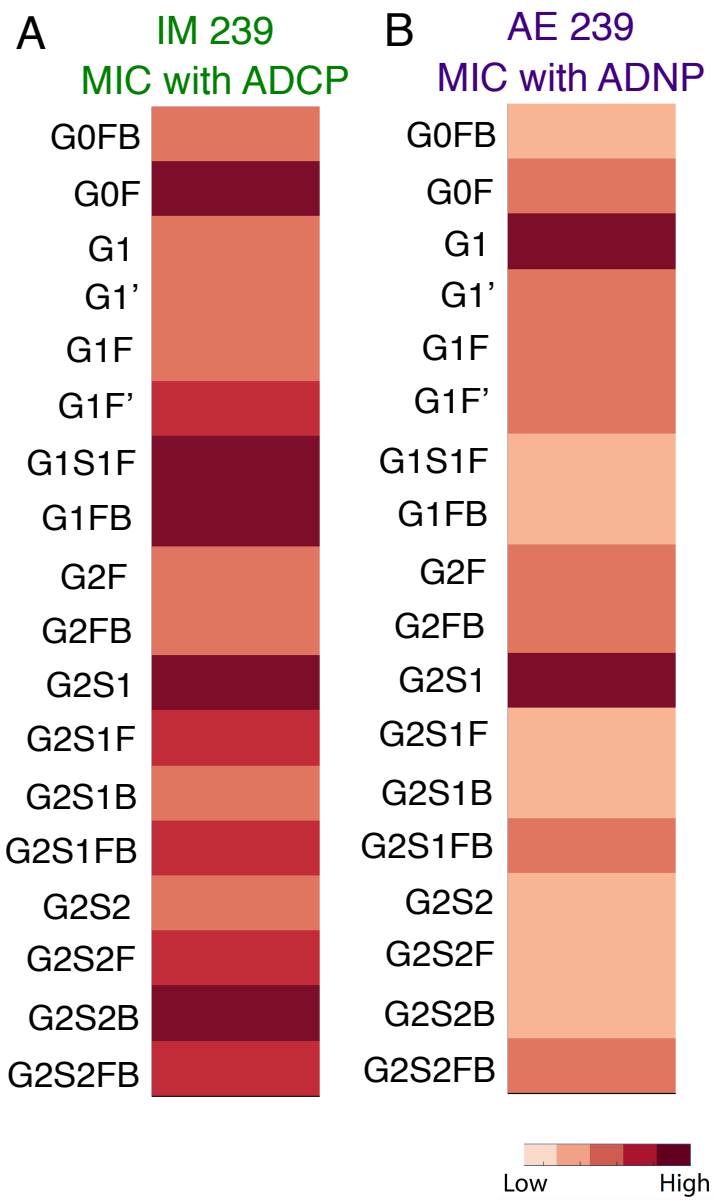

Supplementary Fig. 4. Non-linear relationships between SIV-specific IgG glycoforms and functional correlates. (**A-B**) Maximal information coefficients (MIC) for the IM239 arm between ADCP and individual glycoforms (**A**), and for the AE239 arm between ADNP and individual glycoforms (**B**).

Supplementary Figure 5

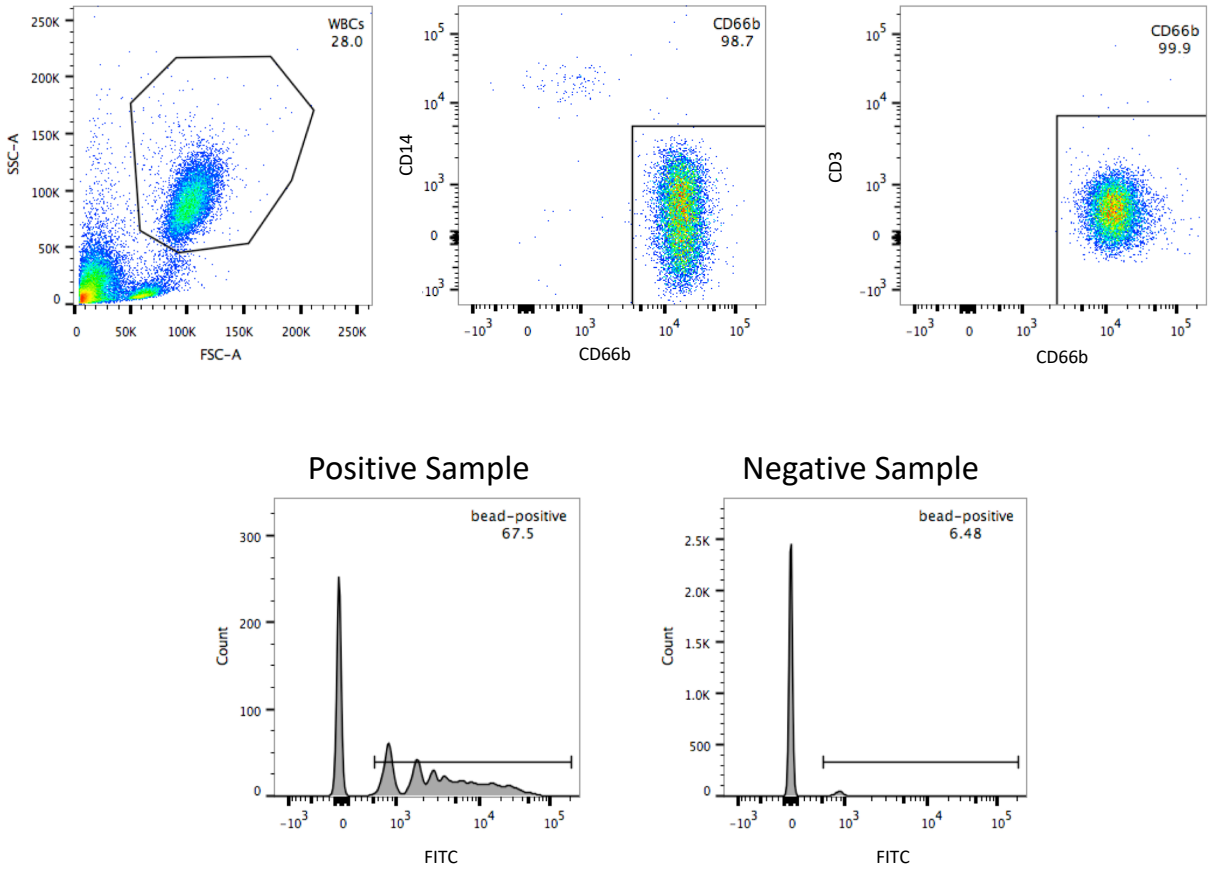

Supplementary Figure 5. Antibody dependent neutrophil phagocytosis gating strategy

Supplementary Figure 6

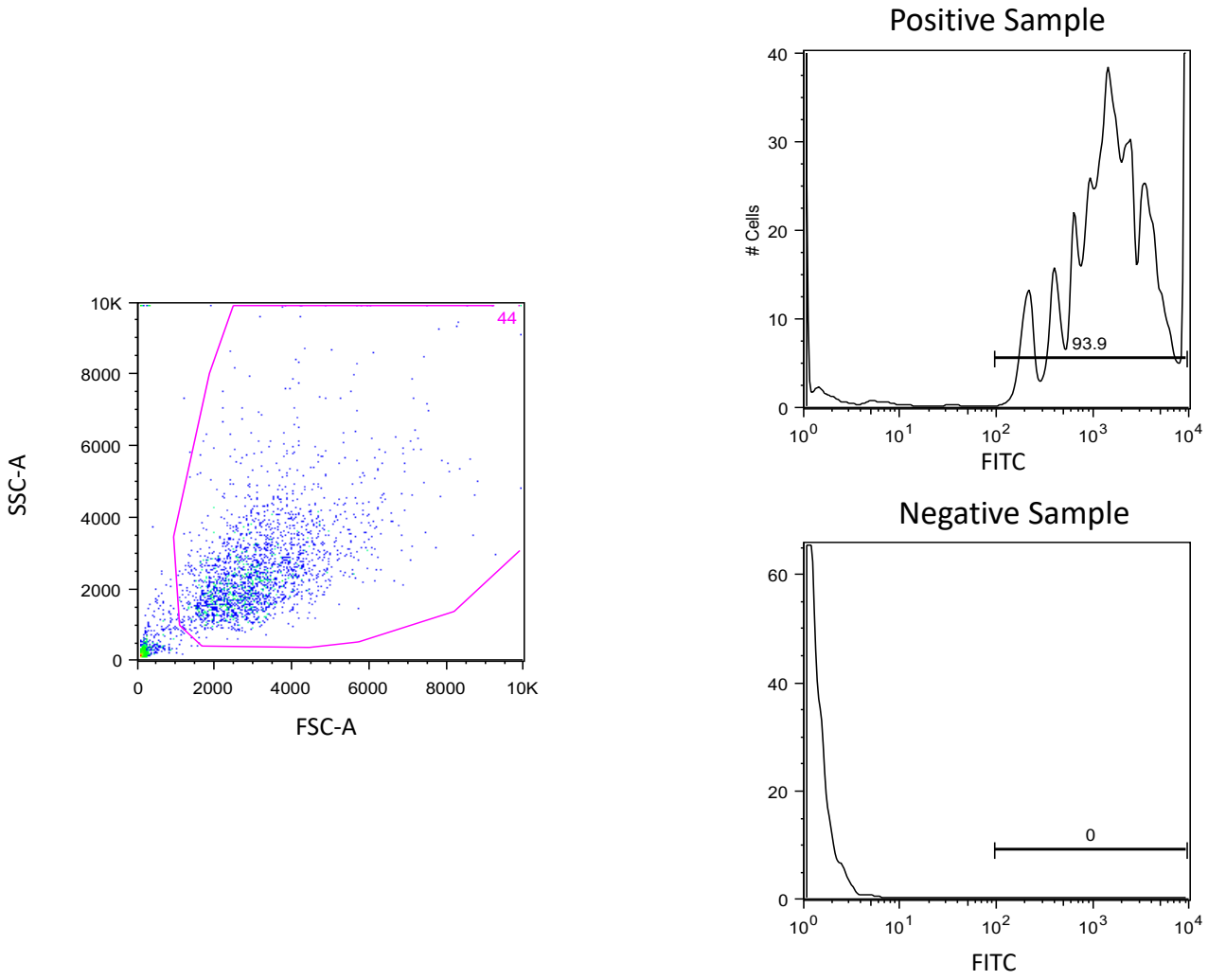

Supplementary Figure 6. Antibody dependent cellular phagocytosis gating strategy

Supplementary Figure 7

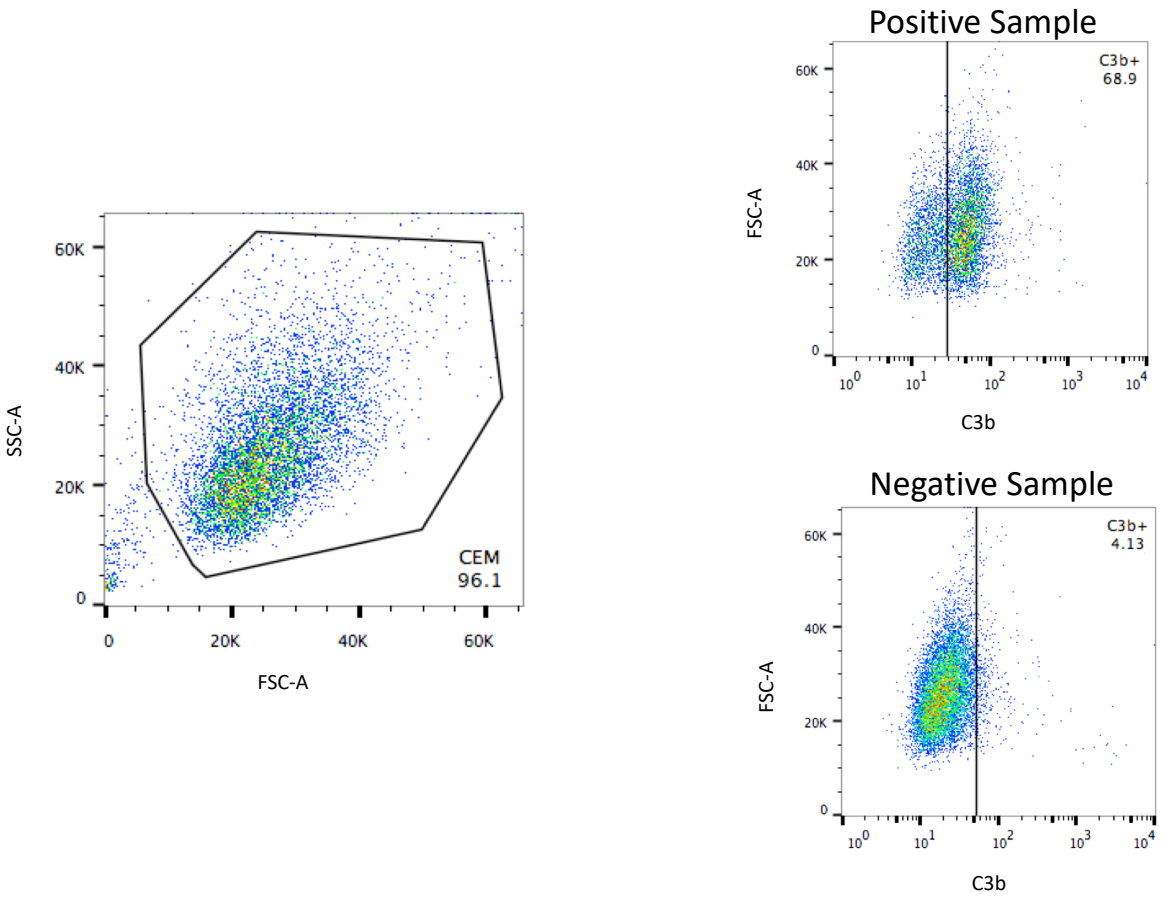

Supplementary Figure 7. Antibody dependent complement deposition gating strategy

Supplementary Figure 8

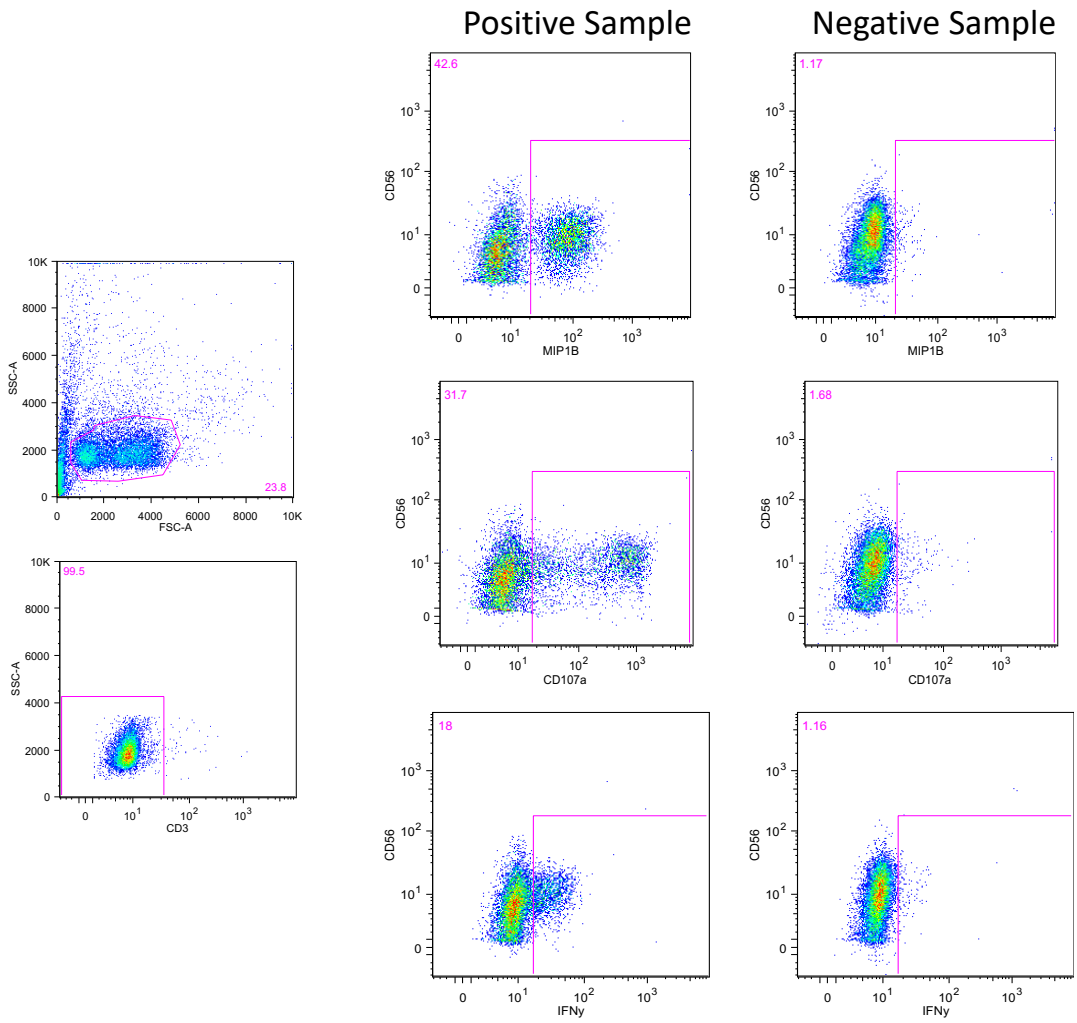

Supplementary Figure 8. Antibody dependent NK cell activation assay gating strategy

Supplementary Figure 9

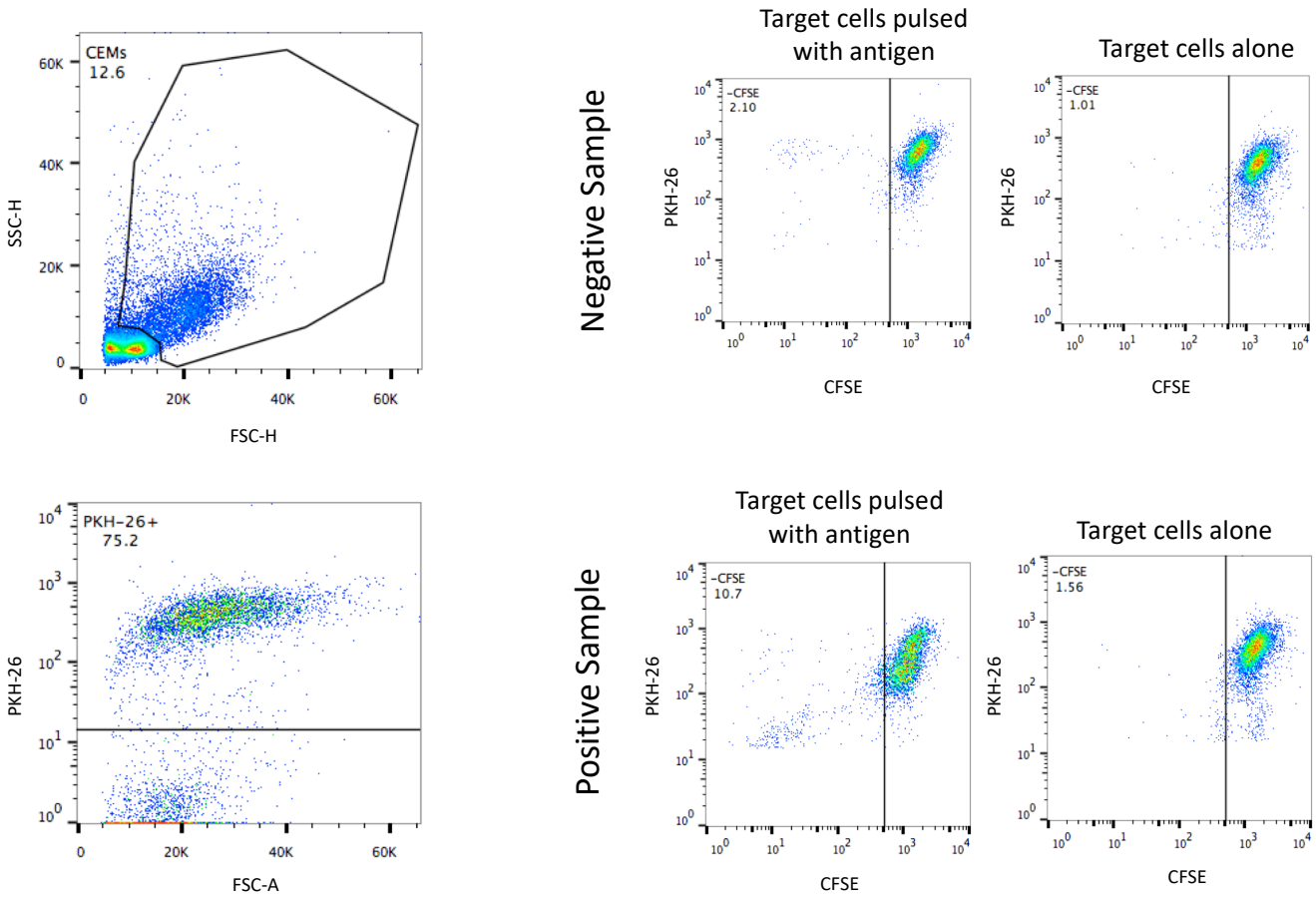

Supplementary Figure 9. Antibody dependent cellular cytotoxicity gating strategy

Supplementary Table 1. Challenge outcomes

Immunogen	Route	Infection Rate	Acquisition Efficacy	Viral Load @ peak (log10)	Viral Load @ Set-point (log10)
Control		34%		6.8	4.4
Mosaic	IM	22%	35% *(0.12)*	5.7 *(p=0.001)*	3.8 *(p=0.16)*
SIVmac239	IM	11%	69% *(p=0.0002)*	6.1 *(p=0.035)*	4.0 *(p=0.40)*
SIVmac239	**AE**	**11%**	**70%** *(p=0.0002)*	**6.5** *(p=0.39)*	**4.8** *(p=0.35)*

Grey font= previously reported data
Black font= newly added data

Previously reported data from: Roederer, M.*, et al.* Immunological and virological mechanisms of vaccine-mediated protection against SIV and HIV. *Nature* 505, 502-508 (2014).

Supplementary Table 2. Humoral response characteristics evaluated.

SIV Antigens	Detection Reagents	Functions	Glycans
gp120 (SIVmac239, SIVcpzEK505, SIVsmE660.2A5, SIVsmE660.84)	Rh.FcgR2A (1,2,3,4)	ADCP	G0 (G0F, G0FB)
gp130 (SIVmac239)	Rh.FcgR3A (1,3)	ADCC	G1, G1' (G1F, G1'F, G1B, G1S1F)
gp140 (SIVmac239 trimer, SIVmac1A11, SIVsmE543)	IgG [High, Low concentrations]	ADNP	G2 (G2F, G2B, G2S1, G2S1F, G2S1B, G2S1FB, G2S2, G2S2F, G2S2B, G2S2FB)
V1a-GGGGRCNKTETDRWGLTRNAGT	Hu.C1q	CD107a	Fucosylated
G49- (V1b peptide) GGGGENVINESNPCIKNNS	Hu.FcgR2A	IFNγ	Bisected
C1.AK-GGGGAWKNATIPLFCATKNRDTWGT	Hu.FcgR3A	MIP1β	Di-Sialylated
C1.TR-GGGGAWKNATIPLFCTTRNRDTWGT	Hu.FcgR3B	ADCD	Mono-Sialylated
G73- C2 peptide GGGGVIQESCDKHYWDAIR	IgA		
G119- C3 peptide GGGGAIQEVKETLVKHPRY			
J08.V1V2.E660.2A5			
J08.V1V2.E660.84			
J08.V1V2.mac239			